Semi-Modal based GW Signal Reconstruction to determine the Peak Frequency

A **Thesis**

Submitted in Partial Fulfilment of the Requirements

for the Degree of **Master of Science**

In

Physics

by

RAHUL E

Roll No: M220585PH

under the supervision of

Dr HARIS MK



DEPARTMENT OF PHYSICS

NATIONAL INSTITUTE OF TECHNOLOGY CALICUT

NIT CAMPUS P.O. - 673601, KOZHIKODE, KERALA, INDIA

MAY 2024

© AUTHOR, (2024)

NIT Calicut has the sole ownership of Patents and Software Copyrights resulting out of this Thesis work. NIT Calicut has the royalty-free permission to reproduce and distribute copies of this Thesis for teaching and research as well as for dissemination of teaching and research in other academic institutions.

I dedicate this thesis to my beloved parents, A ETHIRAJULU and E VATSALA, whose unwavering support and encouragement have empowered me to pursue my passion wholeheartedly.

Acknowledgements

I am deeply grateful to the National Institute of Technology Calicut for granting me the profound opportunity to undertake my master's project journey. My sincere appreciation extends to my esteemed project guide, Dr. Haris M K, whose unwavering support and expert guidance have been a pillar of strength throughout every phase of this endeavour. His wealth of knowledge, profound expertise, and relentless encouragement have been indispensable in shaping the success of this project. I, also, extend my deepest gratitude to my beloved family and supportive friends for their boundless love, unwavering encouragement, and understanding. Their constant motivation served as a beacon of light, fuelling my determination to pursue and achieve my academic aspirations.

RAHUL E

Declaration

I hereby declare that except where specific reference is made to the work of others, the contents of this thesis are original and have not been submitted in whole or in part for consideration for any other degree or qualification in this, or any other university. This thesis is my own work and contains nothing which is the outcome of work done in collaboration with others, except as specified in the text and Acknowledgements.

Signature :
Name : RAHUL E
Roll No : M220585PH

NIT Calicut

*Date :*___/___/_____



Certificate

This is to certify that the M.Sc thesis entitled **Semi-Modal based GW Signal Reconstruction to determine the Peak Frequency.** submitted by **RAHUL E** to National Institute of Technology Calicut for the award of the degree of Master of Science in Physics is a bonafide record of the research work carried out by him under our supervision and guidance. The content of the thesis, in full or parts have not been submitted to any other institute or university for the award of any degree or diploma.

Project Guide
Dr Haris MK
Department Of Physics
NIT Calicut

Faculty Advisor
Dr. Saurabh Gupta
Department Of Physics
NIT Calicut

Place : NIT Calicut

*Date :*___/___/_____

Signature of the Head of the department

(Office Seal)

ABSTRACT

Gravitational waves (GWs) provide invaluable insights into some of the most cataclysmic events in the universe, such as black hole mergers and neutron star collisions. Accurately characterizing GW signals is crucial for understanding the astrophysical phenomena that produce them. In this study, we propose a novel approach utilizing semi-model-dependent reconstruction methods for analyzing GW signals. We leverage posterior samples obtained from parameter estimation techniques to reconstruct GW waveforms and determine peak frequency. Our methodology offers a promising avenue for improving the fidelity of GW signal analysis, particularly in cases where traditional model-dependent approaches may be inadequate. By combining the strengths of parameter estimation and reconstruction methods, we aim to enhance our understanding of GW events and their astrophysical implications. Through comprehensive analysis and interpretation of reconstructed signals, we contribute to the growing body of research aimed at unlocking the secrets of the gravitational wave universe.

Contents

1 Gravitational Waves **1**
1.1 Introduction 1
1.2 Wavelets and Continuous Wavelet Transform 3
1.3 Quasi Model-Dependent Signal Reconstruction 4

2 Signal Reconstruction **6**
2.1 Identifying Essential Wavelets 7
2.2 Optimization of Spectral Loss Parameter (R^*) 7
2.3 Steps to Reconstruct Signal 9

3 Peak Frequency **11**
3.1 Peak Frequency 11

4 Data and Results **13**
4.1 Analysis of Injected Signal 13
4.1.1 Injected Signal 13
4.1.2 Signal Reconstruction 14
4.1.3 h_+ and $h_\times$ Polarization and Phase 15
4.1.4 Peak Frequency 16
4.2 Analysis of Real Signal - GW150914 17
4.2.1 Signal Reconstruction 17
4.2.2 h_+ and $h_\times$ Polarizations 17
4.2.3 Comparison with Theoretical Models 18

References **20**

List of Figures

1.1 The gravitational-wave event GW150914 observed by the LIGO Hanford (H1, left column panel) and Livingston (L1, right column panel) detectors. 2
1.2 A time-frequency map of GW150914, the first detected gravitational wave signal, created using the CWT with Morlet-Gabor wavelets at $Q = 6.0$ and logarithmic frequency spacing. 4

2.1 The noise averaged match $\langle \mathscr{M}_{noise} \rangle$ as a function of spectral loss parameter R^*. The solid dot on the curve indicates its maxima. The right y-axis shows the relative number of essential wavelets ($\overrightarrow{N}_W$) as a function of R^*. 8

4.1 Injectd Signal generated from maximum likelihood parameters. 14
4.2 Waveform generated added with the noise obatained the power spectral denstiy 14
4.3 Reconstructed Signal and Template 15
4.4 h_+ and $h_\times$ polarization values obtained from the reconstructed signal and the template 15
4.5 Phase of the reconstructed signal and the template around the geocenteric time 16
4.6 Time-Frequency plot which shows the match between the reconstructed signal and the template few seconds after the geocenteric time 16
4.7 L1 reconstructed signal along with the template data. 17
4.8 H1 reconstructed signal along with the template data. 18
4.9 h_+ and $h_\times$ Polarizations obtained from the reconstructed signal along with the template 18

Chapter 1

Gravitational Waves

1.1 Introduction

Gravitational waves (GWs) are ripples in the fabric of spacetime, predicted by Albert Einstein's theory of general relativity. These waves are produced by the acceleration of massive objects, such as binary black hole or neutron star systems, and propagate through the universe at the speed of light. Unlike electromagnetic waves, which interact with matter, GWs are able to traverse vast distances across the cosmos without being significantly attenuated or absorbed, making them unique messengers of cosmic events.

The detection of GWs opens a new window into the universe, allowing astronomers to observe phenomena that were previously invisible. GWs provide direct evidence of the most extreme events in the cosmos, such as the collision and merger of black holes and neutron stars, as well as the violent birth of new black holes and neutron stars. By studying GW signals, researchers can investigate the properties of astrophysical objects, test the predictions of general relativity, and probe the nature of spacetime itself.

GWs can be detected using sensitive instruments known as interferometers, which measure tiny changes in the lengths of perpendicular arms caused by passing GWs. The Laser Interferometer Gravitational-Wave Observatory (LIGO), Virgo, and the Kamioka Gravitational Wave Detector (KAGRA) are examples of ground-based interferometers that have successfully detected GWs. Additionally, space-based detec-

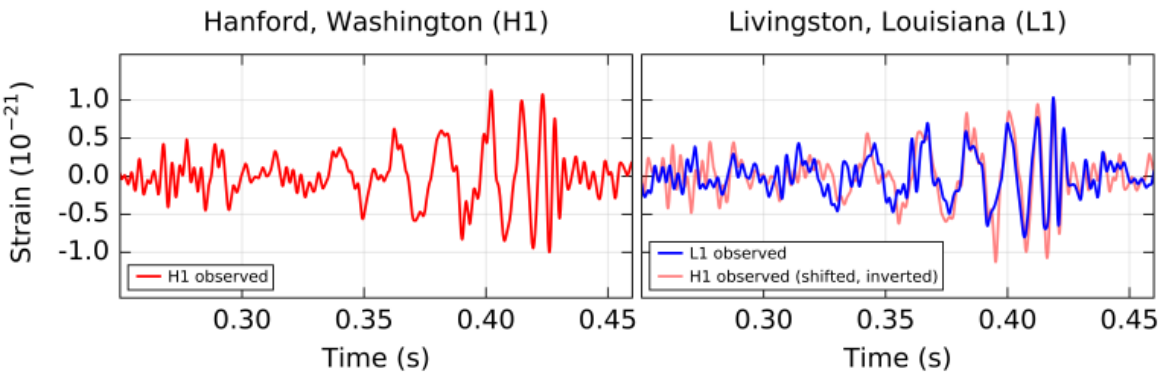


Figure 1.1: The gravitational-wave event GW150914 observed by the LIGO Hanford (H1, left column panel) and Livingston (L1, right column panel) detectors.

tors such as the Laser Interferometer Space Antenna (LISA) are being developed to observe lower frequency GWs from sources such as supermassive black hole mergers.

GW signals exhibit distinct characteristics depending on the nature of the source and the stage of the merger process. The waveform morphology encodes information about the masses, spins, and orbits of the binary system, while the frequency and amplitude of the signal provide insights into the dynamics of the merger. GW signals typically consist of three main phases: inspiral, merger, and ringdown, each characterized by unique frequency modulations and temporal profiles.

Analyzing GW signals involves several sophisticated techniques aimed at extracting meaningful information from noisy data. Parameter estimation methods, such as Bayesian inference, are used to infer the properties of the source, including masses, spins, and distances, by comparing observed signals with theoretical models. Time-frequency analysis techniques, such as Continuous Wavelet Transform (CWT) and Short-Time Fourier Transform (STFT), are employed to characterize the frequency evolution of GW signals and identify transient features. Machine learning algorithms, such as deep neural networks, are also being explored as tools for signal detection,

classification, and denoising in GW data analysis.

1.2 Wavelets and Continuous Wavelet Transform

Gravitational wave (GW) signals, originating from some of the most energetic events in the universe, pose unique challenges for analysis due to their transient nature and dynamic frequency content. Wavelet analysis, particularly through the Continuous Wavelet Transform (CWT), has emerged as a powerful methodology to address these challenges and unlock valuable insights into GW sources. Wavelets are mathematical functions characterized by their ability to capture localized features within signals, making them well-suited for analyzing GW waveforms that exhibit complex frequency modulations over time. In the context of GW analysis, CWT offers a time-frequency representation of the signal, allowing researchers to localize and characterize transient features such as chirps and bursts associated with binary mergers. By convolving the GW signal with a family of scaled and translated wavelet functions, CWT provides a detailed depiction of signal morphology in both time and frequency domains, enabling the identification of distinct phases of a GW event, including the inspiral, merger, and ringdown.

Moreover, CWT facilitates the denoising of GW data by separating signal components from noise and enhancing the signal-to-noise ratio, thereby improving the sensitivity of GW detectors. The versatility of wavelet analysis, coupled with the adaptability of CWT to capture features across multiple scales, makes it an invaluable tool for studying GW signals and unraveling the astrophysical phenomena driving their emission. Through wavelet-based techniques, researchers can gain deeper insights into the properties of GW sources, advancing our understanding of the universe's most extreme events.

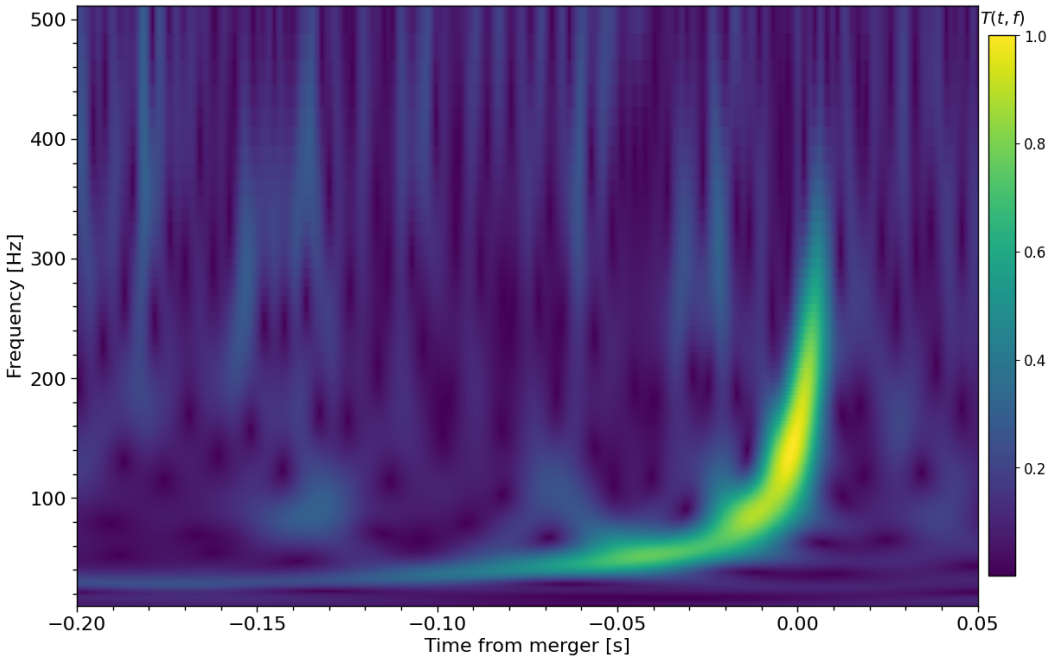


Figure 1.2: A time-frequency map of GW150914, the first detected gravitational wave signal, created using the CWT with Morlet-Gabor wavelets at $Q = 6.0$ and logarithmic frequency spacing.

1.3 Quasi Model-Dependent Signal Reconstruction

We use a quasi model-dependent method for the reconstruction of signals from noisy data, particularly focusing on gravitational waveforms generated by binary black hole mergers. Our approach involves identifying essential wavelets derived from the binary black hole merger waveforms estimated using standard Bayesian analysis techniques. Unlike unmodelled reconstruction methods that identify wavelets coherent across detector networks, our method focuses on selecting wavelets that form coherent clusters in the time-frequency plane, akin to patches with irregular boundaries.

The area covered by these patches directly corresponds to the level of noise persistence in the reconstructed signal. To optimize the placement of wavelets in the time-scale plane, we adopt a dyadic grid placement method, which is known for its

efficiency in constructing an orthonormal wavelet basis. This placement strategy assumes an output of octave decomposition, ensuring a power-of-two logarithmic grid structure. By maintaining sparseness within this grid, we aim to strike a balance between achieving maximum signal representation and minimizing computational costs.

However, finding the optimal level of sparseness is critical. While a highly sparse grid may adequately represent the signal, it could result in larger patch areas, potentially leading to increased noise in the reconstructed signal. Conversely, an overdense grid fails to significantly reduce the patch area beyond a certain limit, while also escalating computational expenses. Therefore, our objective is to achieve maximum sparseness without compromising the fidelity of signal representation, ensuring an efficient and effective reconstruction process.

We utilize log-uniform scale to place the wavelets over the time-scale domain. This scale differs from traditional approaches by offering a logarithmic distribution that ensures wavelets are spaced more densely at lower frequencies and more sparsely at higher frequencies. To complement this scale, we derive an inverse wavelet transformation formula tailored for log-uniform scales, ensuring compatibility with our placement method.

The wavelets generated using log-uniform scales exhibit high redundancy, often termed as over-completeness. While this redundancy may seem counterintuitive, it plays a crucial role in reducing the area covered by essential wavelets. By doing so, we effectively mitigate noise contributions in the reconstructed signal, resulting in a more accurate representation of the underlying signal. The essential wavelets utilizing a log-uniform scale offer a more appropriate representation for high-frequency linear chirp signals, especially those originating from low-mass binary systems.

Chapter 2

Signal Reconstruction

The CWT of a continuous signal $x(t)$ is a linear mapping onto a time-scale space of wavelets [1] :

$$\begin{aligned} X(a,b) &= \int_a^b x(t)\Psi^*_{a,b}(t)\,dt \\ &= \frac{1}{\sqrt{a}}\int x(t)\psi^*\left(\frac{t-b}{a}\right)\,dt \end{aligned} \tag{2.1}$$

where, Ψ^* is the complex conjugate of the shifted and scaled version of the time-localized mother wavelet Ψ, in which a and b are the scale and time-shift parameters, respectively. Therefore, the CWT provides a time-scale representation of the signal by performing a sliding cross-correlation with a continuous family of wavelets. The quantity $1/\sqrt{a}$ outside the integral is an energy normalized factor. It ensures that each wavelet has the same energy, whatever the value of scaling and shift.

The function $\Psi(t)$ must satisfy a set of mathematical criteria to be a wavelet, it must have finite energy[1],

$$E_\psi = \int_\infty^\infty |\psi(t)|^2\,dt < \infty, \tag{2.2}$$

and must hold the admissibility condition[1],

$$C_\psi = \int_\infty^\infty \frac{|\widetilde{\psi}(\omega)|^2}{\omega} d\omega < \infty, \tag{2.3}$$

where, $\widetilde{\psi}(\omega)$ is the Fourier transform of $\psi(t)$, $\omega = 2\pi f$ is the angular frequency, and C_ψ is called the admissibility constant.

2.1 Identifying Essential Wavelets

The conventional method for identifying essential wavelets is a straightforward approach, where one discards the low-magnitude wavelet coefficients by applying a threshold, which is known as wavelet thresholding. This approach aims to remove the noise from data without affecting the basic features of the signal. Here, we employ the modelled waveforms that are obtained from the standard Bayesian parameter estimation analysis. We compute wavelet coefficients for a waveform and set a threshold on coefficient value to select the essential wavelets. The threshold is chosen such that the resultant power from the essential wavelets is equal to a percentage of total power of the spectrogram. We calculate the threshold (E^*) for a given value of fractionalpower loss (R^*) by solving an equation[1],

$$R_* \;=\; 1 - \sum_{n,j} |X(n,j)|^2 \; [|X(n,j)|^2 \geq E_*] \;\Big/\; \sum_{n,j} |X(n,j)|^2 \tag{2.4}$$

We shall call that (R^*) is the spectral loss parameter. As the number of essential wavelets is considerably fewer than the total number of wavelets, a significant amount of noise can be removed while preserving the basic features of the signal.

2.2 Optimization of Spectral Loss Parameter (R^*)

We estimate the performance of the reconstruction methods for gravitational wave signals from compact binary mergers of equal mass non-spinning black holes. For each case, an identical signal is injected in many noise realizations of stationary Gaussian distribution weighted by Advanced LIGO zero-detuned high-power (aLIGO) design sensitivity.

A whiten Gaussian noise is considered to be distributed normally over time-scale domain. This implies that the noise energy is equally distributed over time-scale

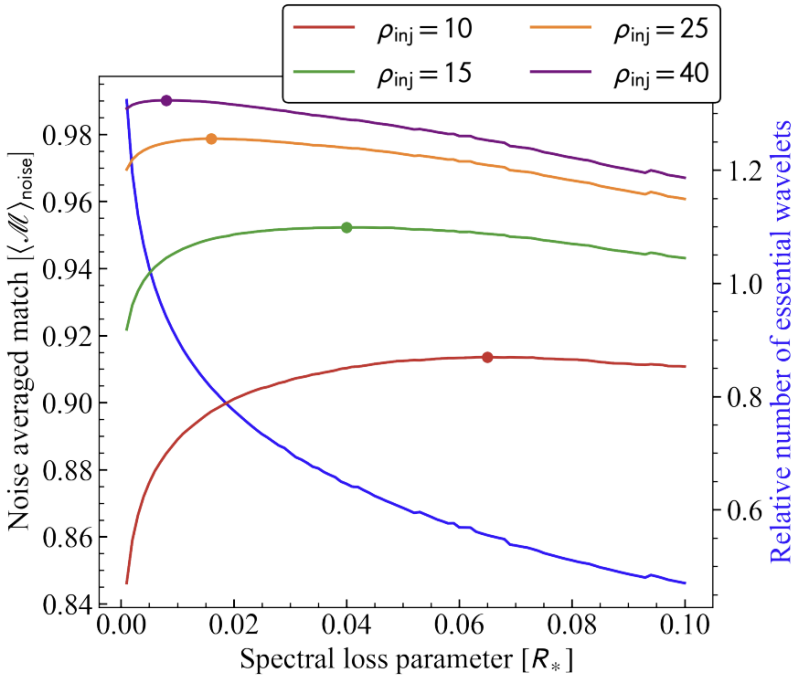


Figure 2.1: The noise averaged match $\langle \mathscr{M}_{noise} \rangle$ as a function of spectral loss parameter R^*. The solid dot on the curve indicates its maxima. The right y-axis shows the relative number of essential wavelets $(\overrightarrow{N}_W)$ as a function of R^*.

domain. The amount of noise retains in the reconstructed signal is determined by the spectral loss parameter (R^*). A higher value of (R^*) can further reduce the inseparable noise in the reconstructed signal. At the same time, the essential wavelets would not be able to represent the complete signal characteristics. It implies that the spectral loss parameter plays a role that imposes a limitation on achieving the maximum overlap between the injected and reconstructed signal. Therefore, we want to optimize this parameter. For a given source parameter and injected SNR, we perform the injection analysis with a set of (R^*) values. The noise averaged match for a given injected signal $h_{inj}(\overline{\lambda}, \rho_{inj})$ and (R^*) can be defined as[1],

$$\langle \mathscr{M}(R^*) \rangle_{noise} = \frac{1}{N} \sum_{i=1}^{N} \mathscr{M}(h_{inj}, h_{rec}[n_i]) \tag{2.5}$$

where, $h_{rec}[n_i]$ represents the reconstructed signal from the data of i^{th} noise realization n_i. To determine the essential wavelets for a given value of R^*, we compute the wavelet coefficients of whitened waveform and plug in to Eq. 2.4.

Fig. 2.1 shows the noise averaged match as a function of R^* for a set of injected SNR values and the number of essential wavelets as a function of R^*. If we fix the spectral loss parameter and increase the injected SNR, the signal contribution to each essential wavelet increases. At the same time, the average noise contribution remains the same since the number of essential wavelets and their properties does not change. This leads to an improvement in the reconstruction accuracy. A fixed SNR curve in the Fig. 2.1 indicates that a smaller value of R^* allows many nonessential wavelets in the analysis. The signal contribution to those wavelets is trivial, but the inseparable noise in the reconstructed signal increases. On the other hand, a higher value of R^* discards many moderate essential wavelets. Thus, the choice of R^* is a tradeoff between the signal and noise contributions to the wavelets. To find an optimum value R, we maximize the quantity $\langle \mathscr{M}(R^*) \rangle_{noise}$ over R^*.

2.3 Steps to Reconstruct Signal

In order to reconstruct the signal from data stream, we follow these steps[1]:

1. For each posterior sample, we generate the CBC template waveform in the detector frame. Since the GR allows only two polarization states, referred to as the plus (h_+) and cross ($h_\times$), the time-domain response $h_I(t)$ of a given detector I is determined by the antenna response functions ($F_{\mathcal{I}}^+$ and $F_{\mathcal{I}}^\times$) of those polarizations,

$$\begin{aligned} h_{\mathcal{I}}(t) = F_{\mathcal{I}}^+(\alpha, \delta, \psi, t) h_\times(t - \Delta t_{\mathcal{I}}; D_L, \iota, \overrightarrow{\lambda}) + \\ F_{\mathcal{I}}^\times(\alpha, \delta, \psi, t) h_+(t - \Delta t_{\mathcal{I}}; D_L, \iota, \overrightarrow{\lambda}) \end{aligned} \tag{2.6}$$

where, α and δ refers to the source sky location in terms of right ascension and declination, ψ is the polarization angle, D_L is the luminosity distance to the source, ι is the inclination angle of the binary plane, $\overrightarrow{\lambda}$ represents the set of intrinsic parameters of the binary system, and $\Delta t_{\mathcal{I}} (\equiv \Delta t_{\mathcal{I}}(\alpha, \delta, t))$ is the travel time of the signal from geocenter to the detector.

2. Whiten the waveform weighted by the noise amplitude spectral density such that the norm of the whitened waveform is equal to its optimal SNR.

3. Compute the wavelet coefficients for each whiten template waveform using the CWT as shown in Eq. 2.1, where wavelets are constructed using the log-uniform scale.

4. Determine the essential wavelets using Eq. 2.4, where spectral loss parameter R^* is obtained from Eq. 2.5. We inject the best fit template (corresponds to maximum likelihood sample) waveform in many simulated noise realizations and estimate the value of R^* for each detector's data. We have found the value of R^* for H1, L1, and V1 is 2.5%, 4%, and 5%, respectively. Please note that we estimate the spectral loss parameter for the maximum likelihood sample and use that value for all the posterior samples.

5. Use those essential wavelets to reconstruct the signal from detector strain.

The above-described procedure is used to obtain a reconstructed signal for each posterior sample. These wavelet-based reconstructed signals are very similar, and their 90% interval is very thin and looks like a line. Therefore, we illustrate the median of reconstructed signals at every time index.

Chapter 3

Peak Frequency

Peak and ringdown frequencies play pivotal roles in characterizing the distinct phases of a GW signal, particularly those emitted by binary black hole or neutron star mergers.

3.1 Peak Frequency

The peak frequency refers to the frequency at which the GW signal exhibits its highest amplitude during the inspiral phase of the binary merger. As two compact objects, such as black holes or neutron stars, spiral towards each other, they emit GWs at increasingly higher frequencies, resulting in a characteristic chirping signal. The peak frequency corresponds to the moment when the inspiral phase culminates, typically marking the onset of the merger phase. Determining the peak frequency is essential for constraining the masses and spins of the binary components, as it provides crucial information about the orbital dynamics and evolution of the system.

GR predicts that GWs of astrophysical interest have two independent polarizations, namely (h_+,$h_\times$). In GR, the instantaneous frequency of the gravitational radiation emitted by a binary is an observable which, given a model for the emission, can be computed as [2]

$$f(t) = \frac{1}{2\pi}\frac{d}{dt}\left(\arg(h_+ - ih_\times)\right) \tag{3.1}$$

Of particular interest is f^{peak}, the frequency of the signal at the time at which the strain amplitude, defined here as $\sqrt{h_+^2 + h_\times^2}$, reaches its peak. This stage approxi-

mately coincides with the time when the two black holes merge, so that f^{peak} peak encodes information on the behavior of the system in the genuine strong-field regime.

To determine the Peak frequency:

1. Reconstruct the signal with essential wavelets by following the steps mentioned in the previously.

2. The reconstructed signal is initially whitened for analysis. To determine the peak frequency (f^{peak}), the signal must be unwhitened. Unwhitening involves taking the FFT of the signal and multiplying it by the square root of its Power Spectral Density (PSD), this quantity is called the Amplitude Power Spectral Density (APSD). This process restores the original signal amplitude characteristics, enabling accurate determination of f^{peak}

3. To account for time shifts from the geo-center for detectors $H1$ and $L1$, adjustments are made during signal analysis. These adjustments correct for the temporal differences between signals received at different locations, ensuring accurate synchronization and alignment for precise analysis and interpretation..

4. Calculate the h_+ and $h_\times$ values from the waveform using Eq 2.6

5. Using Eq 3.1 peak frequency is calculated

Chapter 4

Data and Results

4.1 Analysis of Injected Signal

I obtained the posterior samples from Bilby's reanalysis of GWTC-1[3] and Power Spectral Density files were generated from Pycbc module[4], specifically the Advance 04 Intermediate noise. We generated waveform with the maximum likelihood parameters obtained from the posterior samples file. This is the injected signal. Added noise, generated from the Power Spectral Density files to the wave form.

The signal was reconstructed based on the steps mentioned in section 3, with the maximum likelihood parameter. With the reconstructed signal h_+ and $h_\times$ values were calculated. From which the peak frequency F_{peak} is calculated using the Eq 3.1 mentioned in section 3.

4.1.1 Injected Signal

The Injected signal generated from the maximum likelihood parameter of the posterior sample file is Fig 4.1. The wave form is generated using the function $gen_td_waveform$ function in the QMWaves reconstruct signal pipeline[1]. Resized appropriately with zeros to save it as the frame file to be used for signal reconstruction.

The Injected signal with noise is shown in Fig 4.2. The waveform generated is added to the noise obtained from the power spectral density from Advance 04 Intermediate noise[4].

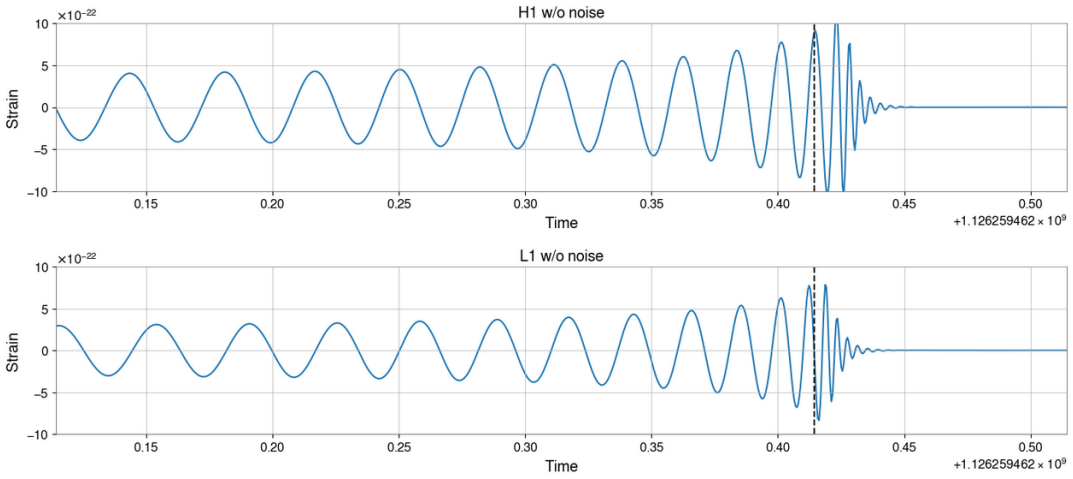


Figure 4.1: Injectd Signal generated from maximum likelihood parameters.

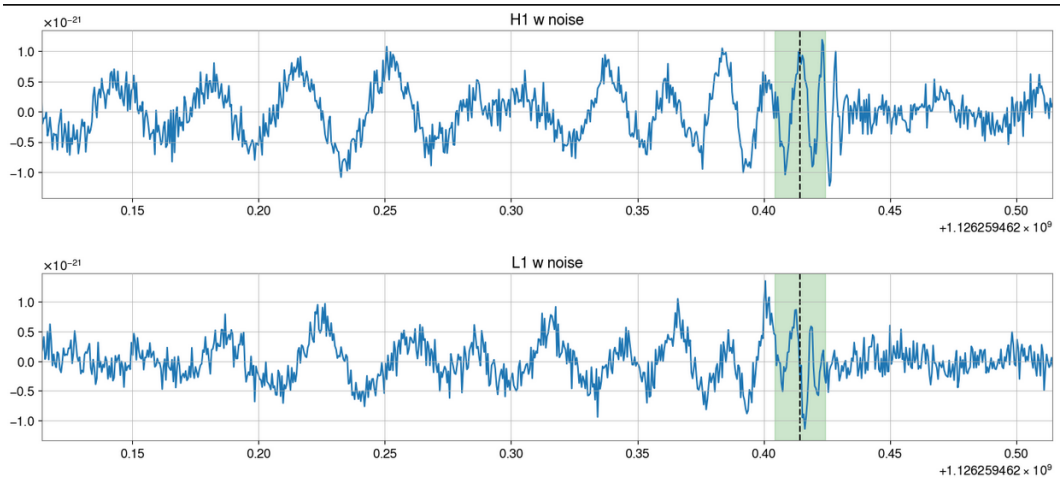


Figure 4.2: Waveform generated added with the noise obatained the power spectral denstiy

4.1.2 Signal Reconstruction

The Signal is reconstructed with the injected signal as the frame file, psd obtained the Advance 04 Intermediate noise, and using the template generated from the posterior samples. The reconstructed signal along with template is shown in Fig 4.3.

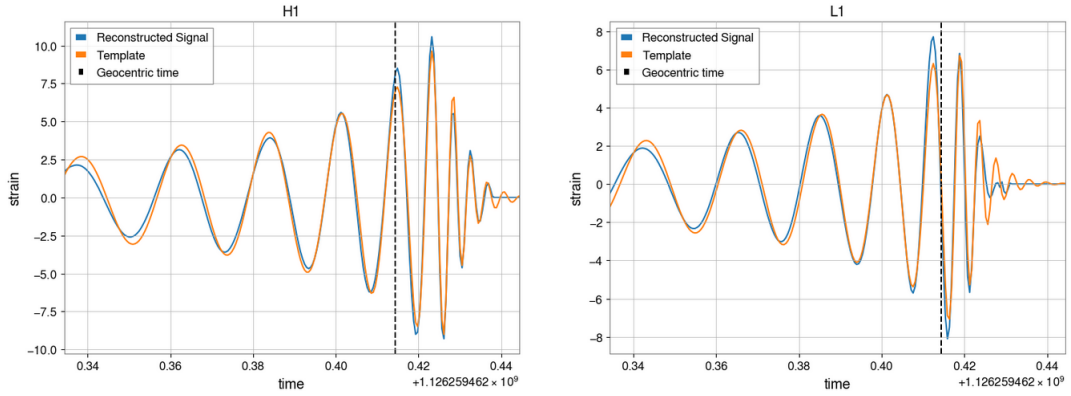


Figure 4.3: Reconstructed Signal and Template

4.1.3 h_+ and $h_\times$ Polarization and Phase

The Reconstructed signal and the template is unwhitened using the Amplitude power spectral density obtained from the power spectral density. The unwhitened reconstructed signal and template is used to calculate the h_+ and $h_\times$ polarizations, which is necessary to calculate the peak frequency F_{peak}. The Fig 4.4

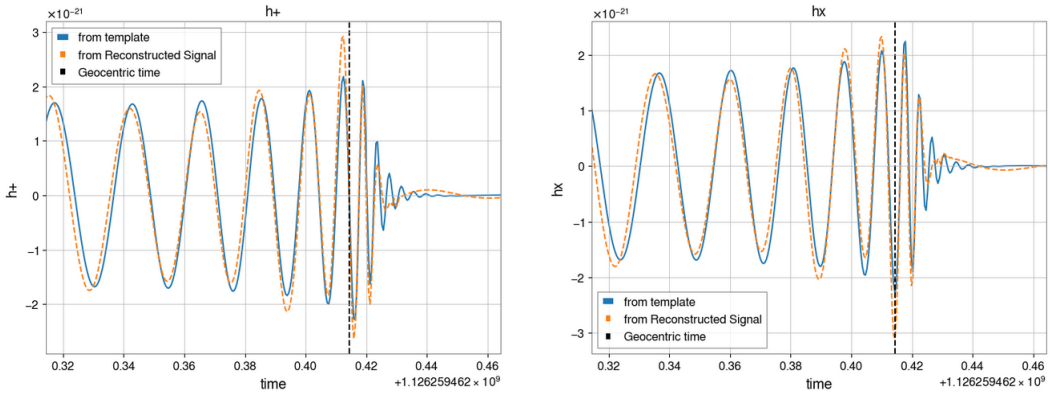


Figure 4.4: h_+ and $h_\times$ polarization values obtained from the reconstructed signal and the template

The h_+ and $h_\times$ polarizations are used to calculate the phase of the signal. The Fig 4.5 shows the phase of the signal around the geocentric time because that is the region important, in the context of the peak frequency calculation.

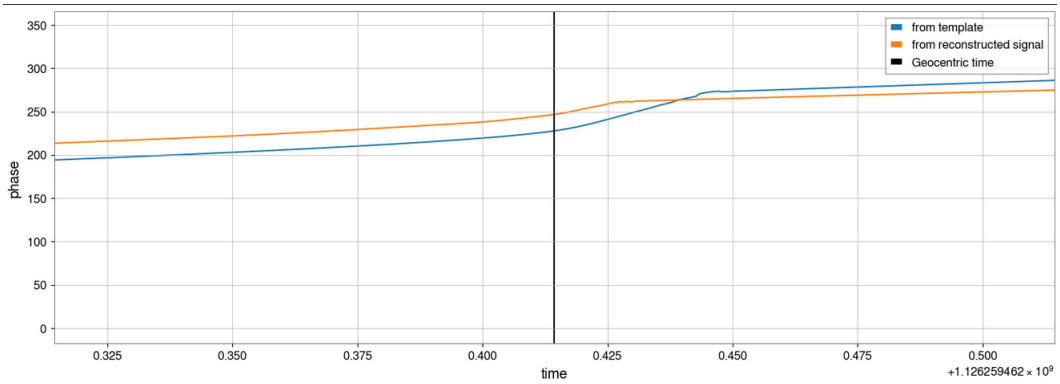


Figure 4.5: Phase of the reconstructed signal and the template around the geocenteric time

4.1.4 Peak Frequency

Finally with the peak frequency is calculated using the h_+ and $h_\times$ polarization values and the phase values using the Eq. 3.1. The Fig 4.6 shows the time frequency scatter plot of the reconstructed signal and the template which is almost close to each other.

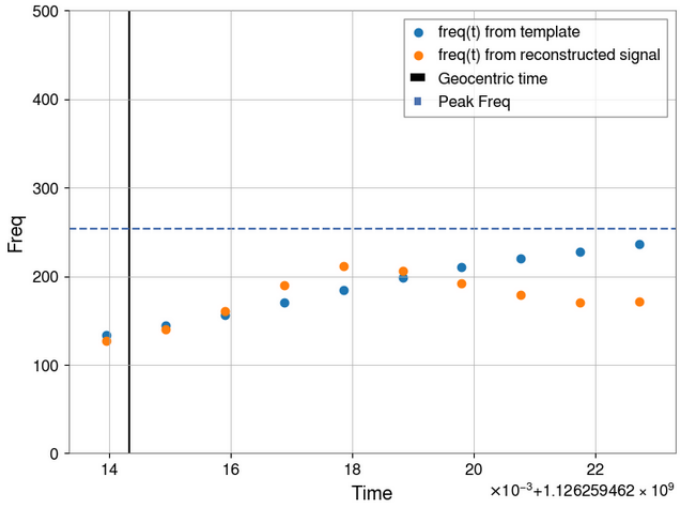


Figure 4.6: Time-Frequency plot which shows the match between the reconstructed signal and the template few seconds after the geocenteric time

4.2 Analysis of Real Signal - GW150914

The 2^{nd} part of the project began with the utilization of real event GW150914, with data obtained from GW Open Science Center.

4.2.1 Signal Reconstruction

The L1 (Fig 4.1) and H1 (Fig 4.2) strain data is reconstructed using the essential wavelets, based on the steps mentioned in section 2.

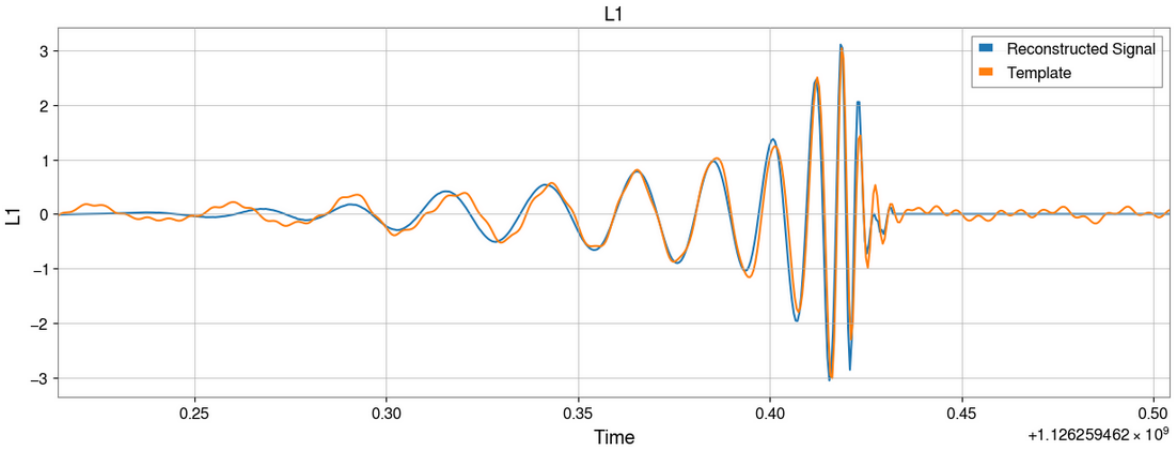


Figure 4.7: L1 reconstructed signal along with the template data.

4.2.2 h_+ and $h_\times$ Polarizations

Following the successful reconstruction of the signals from L1 and H1, the h+ and hx polarizations were reconstructed and compared with the theoretical predictions based on templates.

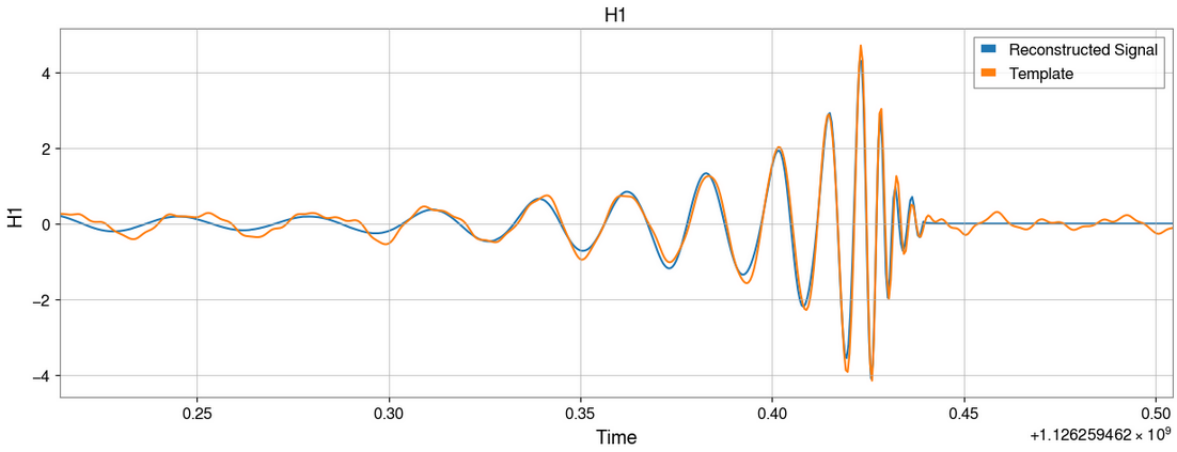


Figure 4.8: H1 reconstructed signal along with the template data.

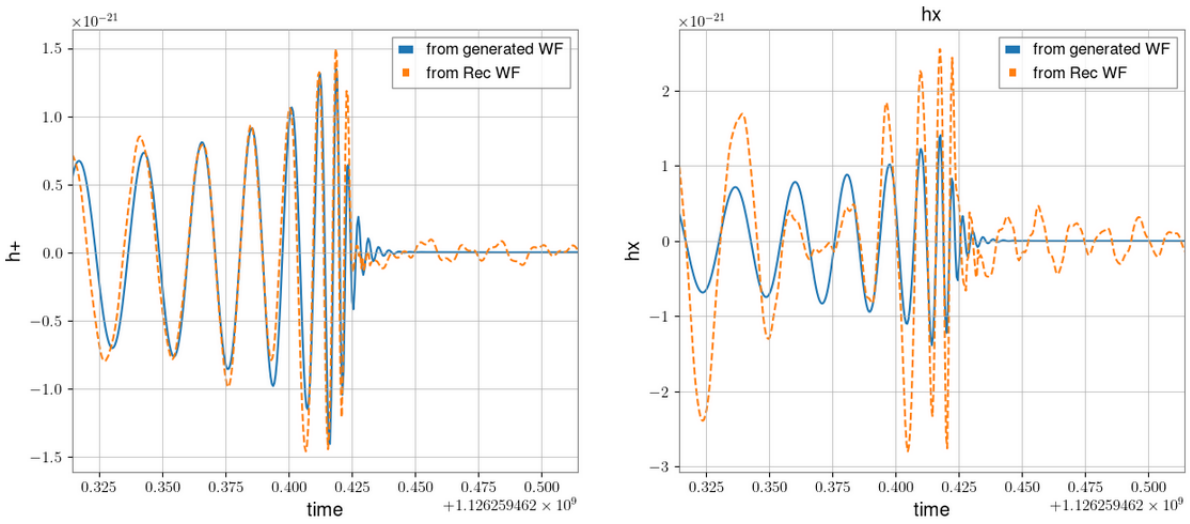


Figure 4.9: h_+ and $h_\times$ Polarizations obtained from the reconstructed signal along with the template

4.2.3 Comparison with Theoretical Models

Plots showcasing the reconstructed h_+ and $h_\times$ polarizations were generated and compared against the expected values calculated from the theoretical templates. It was observed that the reconstruction quality for the $h_\times$ polarization was significantly

poorer compared to h_+. Despite GW150914 being a high signal-to-noise ratio (SNR) event, the challenges in accurately reconstructing $h_\times$ were noted and further analyzed. Due to this poor reconstruction quality, accurate calculation of the peak frequency of the GW150914 event using the $h_\times$ polarization was not feasible.

References

1.Soumen Roy, **Nonorthogonal wavelet transformation for reconstructing gravitational wave signals**, url: http://dx.doi.org/10.1103/PhysRevResearch.4.033078, DOI : 10.1103/physrevresearch.4.033078, Journal: Physical Review Research, Publisher: American Physical Society (APS), 2022

2.Carullo, Gregorio and Riemenschneider, *et.al* , **GW150914 peak frequency: a novel consistency test of strong-field general relativity**, url: http://dx.doi.org/10.1088/1361-6382/ab185e, DOI : 10.1088/1361-6382/ab185e, Journal: Classical and Quantum Gravity, Publisher: IOP Publishing, 2019

3.**Bilby's reanalysis of GWTC-1**, url:https://bilby-gwtc1.github.io

4.**PyCBC: Powering Gravitational-wave Astronomy**, url: https://pycbc.org/pycbc/latest/html

5.M K Haris, PhD Thesis, **Gravitational wave multi-detector schemes for compact binary coalescence search**, Institute: Indian Institute of Science Education and Research Thiruvananthapuram, Month: October, Year: 2016

6.Jolien D. E. Creighton and Warren G. Anderson, Book: **Gravitational-Wave Physics and Astronomy: An Introduction to Theory, Experiment and Data Analysis and Astronomy**, Publisher: WILEY-VCH, Year:2011

7.**GWpy 3.0.8 documentation**, url: https://gwpy.github.io/docs/stable/

8.Klimenko, S. and Mitselmakher, Guenakh, **A wavelet method for detection of gravitational wave bursts**, doi = 10.1088/0264-9381/21/20/025, Journal: Class. Quant. Grav, Year: 2004

9.B. P. Abbott et al.*, **Observation of Gravitational Waves from a Binary Black Hole Merger**, DOI: 10.1103/PhysRevLett.116.061102, Journal: PHYSICAL REVIEW LETTERS, Year:2016)